Pyrido[1,2-*a*]pyrimidin-4-one Derivatives as a Novel Class of Selective Aldose Reductase Inhibitors Exhibiting Antioxidant Activity

Concettina La Motta,*[,†] Stefania Sartini,[†] Laura Mugnaini,[†] Francesca Simorini,[†] Sabrina Taliani,[†] Silvia Salerno,[†] Anna Maria Marini,[†] Federico Da Settimo,[†] Antonio Lavecchia,*[,§] Ettore Novellino,[§] Miriam Cantore,[‡] Paola Failli,[‡] and Mario Ciuffi[‡]

Dipartimento di Scienze Farmaceutiche, Università di Pisa, Via Bonanno 6, 56126 Pisa, Italy, Dipartimento di Chimica Farmaceutica e Tossicologica, Università di Napoli "Federico II", Via D. Montesano, 49, 80131 Napoli, Italy, Dipartimento di Farmacologia Preclinica e Clinica, Università di Firenze, Viale Pieraccini 6, 50139 Firenze, Italy

Received April 4, 2007

2-Phenyl-pyrido[1,2-*a*]pyrimidin-4-one derivatives bearing a phenol or a catechol moiety in position 2 were tested as aldose reductase (ALR2) inhibitors and exhibited activity levels in the micromolar/submicromolar range. Introduction of a hydroxy group in position 6 or 9 gave an enhancement of the inhibitory potency (compare **18**, **19**, **28**, and **29** vs **13** and **14**). Lengthening of the 2-side chain to benzyl determined a general reduction in activity. The lack or the methylation of the phenol or catechol hydroxyls gave inactive (**10**−**12**, **21**, **22**, **25**−**27**) or scarcely active (**15**, **17**, **20**) compounds, thus demonstrating that the phenol or catechol hydroxyls are involved in the enzyme pharmacophoric recognition. Moreover, all the pyridopyrimidinones displayed significant antioxidant properties, with the best activity shown by the catechol derivatives. The theoretical binding mode of the most active compounds obtained by docking simulations into the ALR2 crystal structure was fully consistent with the structure−activity relationships in the pyrido[1,2-*a*]pyrimidin-4-one series.

Introduction

Diabetes mellitus is a metabolic disorder characterized by high levels of blood glucose, resulting from defects in insulin production, insulin action, or both. It is recognized as a public health problem, as it affects a significant portion of the population worldwide and is rising to pandemic proportions. According to epidemiological studies, approximately 135 million adults worldwide were diagnosed with diabetes in 1995, and this number is expected to rise to at least 300 million by 2025, with a 122% overall increase in the worldwide prevalence.[1−5]

Diabetes is a lifelong condition that seriously affects a person's quality of life. It can be successfully controlled by the administration of insulin and potent oral hypoglycemics, but it still remains the cause of significant morbidity and mortality due to a progressive development of disabling complications. Patients with diabetes are at a higher risk for cardiovascular events, including strokes, and show accelerated formation of severe atherosclerotic lesions in peripheral, coronary, and cerebral arteries. They quickly develop visual impairment and blindness due to cataracts and severe retinopathy, as well as terminal renal diseases and different forms of nervous system damage, including an impaired sensation of pain and physical disability.[6,7]

The high and rising incidence of diabetes, its impact on morbidity and mortality, and its high human and economic costs clearly establish the prevention of this disease as an urgent priority for national and international health authorities. While research on the prevention of diabetes itself is promising,[8,9] preventing the onset of the chronic biochemical and functional alterations occurring in response to diabetic hyperglycemia is still unfruitful. Different clinical studies[10,11] demonstrate that close control of blood glucose is significantly effective in reducing these alterations, but even an optimal control of blood glucose could not prevent their onset, suggesting that alternative strategies are needed.

Experimental and clinical evidence demonstrates that the pathogenic mechanism leading to diabetic complications is causally linked to an increased activity of the enzyme aldose reductase (alditol/$NADP^+$ [a] oxidoreductase, EC 1.1.1.21, ALR2). This is the first enzyme of the polyol pathway and catalyzes the NADPH-dependent reduction of glucose to sorbitol, which is then oxidized to fructose by sorbitol dehydrogenase (L-iditol/NAD^+, 5-oxidoreductase, EC 1.1.1.14, SD). As ALR2 has a low substrate affinity for glucose, the conversion of glucose to sorbitol is generally nonsignificant in normoglycemic conditions. In fact, ALR2 must compete directly with the hexokinase of the glycolytic pathway for the utilization of glucose, and as the substrate affinity of hexokinase is greater than that of ALR2, glucose is preferentially phosphorylated with ATP by this enzyme. Under hyperglycemic conditions, hexokinase is rapidly saturated and the polyol pathway becomes activated. Sorbitol is formed more rapidly than it is converted to fructose, and its polarity hinders its penetration through membranes and subsequent removal from tissues by diffusion. The resulting elevated

* To whom all correspondence should be addressed. Tel.: (+)-390502219593 (C.L.M.); (+)39081678613 (A.L.V.). Fax: (+)390502219605 (C.L.M.); (+)39081678613 (A.L.V.). E-mail: lamotta@farm.unipi.it (C.L.M.); lavecchi@unina.it (A.L.V.).

† Dipartimento di Scienze Farmaceutiche, Università di Pisa.

§ Dipartimento di Chimica Farmaceutica e Tossicologica, Università "Federico II" di Napoli.

‡ Dipartimento di Farmacologia Preclinica e Clinica, Università di Firenze.

[a] Abbreviations: PPP, 2-phenylpyrido[1,2-*a*]pyrimidin-4-one; ALR2, aldose reductase; ALR1, aldehyde reductase; ARI, aldose reductase inhibitor; NADPH, β-nicotinamide adenine dinucleotide phosphate reduced form; $NADP^+$, β-nicotinamide adenine dinucleotide phosphate; NADH, β-nicotinamide adenine dinucleotide reduced form; NAD^+, β-nicotinamide adenine dinucleotide; SD, sorbitol dehydrogenase; ATP, adenosine triphosphate; ROS, reactive oxygen species; PKC, protein kinase C; MAPK, mitogen-activated protein kinase; PARP, poly(ADP-ribose)polymerase; HNE, hydroxynonenal; AKR, aldo-keto reductase; PPA, polyphosphoric acid; TBARS, thiobarbituric acid reactive substances; MD, molecular dynamics; SAR, structure−activity relationship; MDA, malondialdehyde.

10.1021/jm070398a CCC: $37.00
Published on Web 09/11/2007

Chart 1. Aldose Reductase Inhibitors

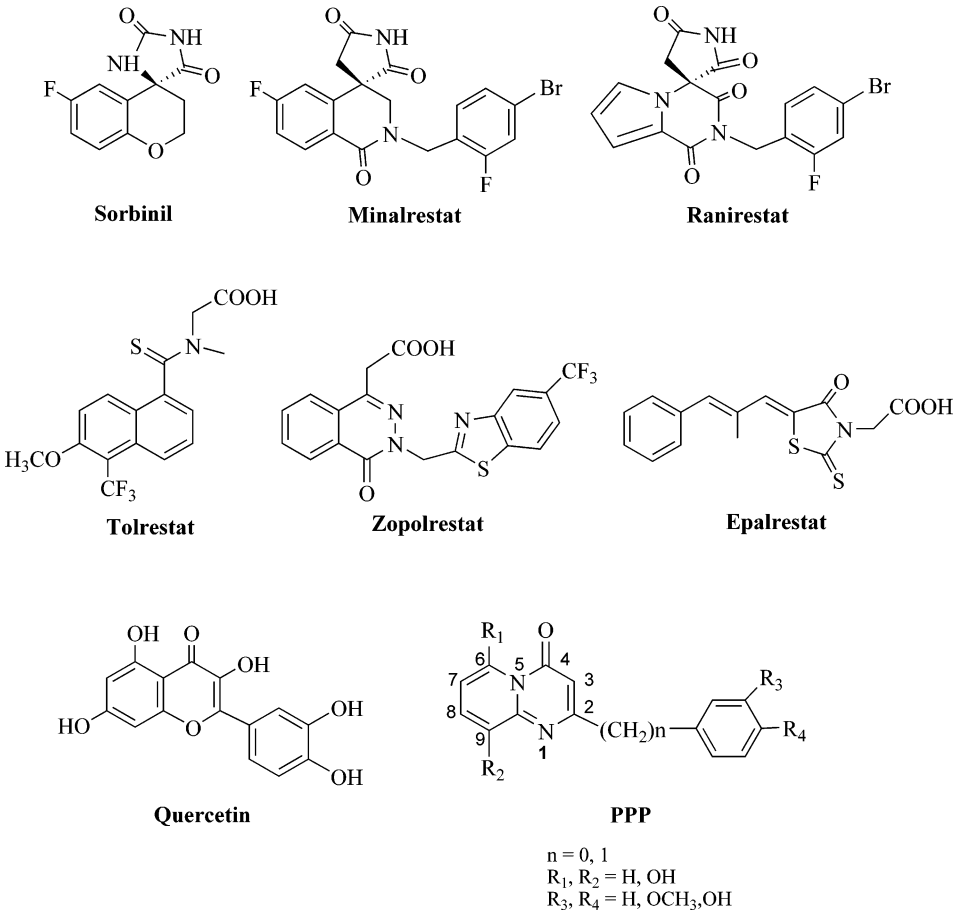

intracellular concentration of sorbitol increases cellular osmolarity, which in turn initiates a cascade of events that lead to the development of long-term diabetic complications.[12−14]

In addition to the osmotic imbalance, an increase in the activity of the polyol pathway during hyperglycemia causes a substantial imbalance in the free cytosolic coenzyme ratios $NADPH/NADP^+$ and $NAD^+/NADH$. This alteration in the redox state of pyridine nucleotides induces a state of pseudohypoxia, which contributes to the onset of hyperglycemic oxidative stress through the accumulation of reactive oxygen species (ROS). ROS, in turn, trigger activation of downstream mechanisms, namely, protein kinase C (PKC) isoforms, mitogen-activated protein kinases (MAPKs), and poly(ADP-ribose)-polymerase (PARP), as well as the inflammatory cascade, which sustains the pathogenesis of diabetic complications.[15−19] Furthermore, the increase in fructose levels connected with the polyol pathway activation accelerates the development of these complications, because fructose and its metabolites are almost 10 times more potent nonenzymatic glycation agents than glucose.

Besides these biochemical evaluations, newer approaches involving genetic analysis conducted on transgenic and knockout mice provide unambiguous evidence of the role of ALR2 in the development of diabetic complications. Recent studies also clearly demonstrate a correlation between overexpression of the human ALR2 gene and the likelihood of the development of complications among diabetic patients.[20]

Inhibition of ALR2 is therefore a useful therapeutic strategy to prevent the onset, or at least delay, the progression and the severity of diabetic complications.

Many structurally different compounds have been shown to inhibit this enzyme with various degrees of efficacy and specificity (Chart 1). However, none of them but epalrestat are currently marketed. Products that appear to be promising during in vitro studies or in trials with animal models often fail to proceed any further either because of undesirable side effects or as a result of poor efficacy. These effects are mainly due to a lack of selectivity for other enzymes, especially the closely related aldehyde reductase (EC 1.1.1.2, ALR1). ALR1 is ubiquitously present in all tissues and plays a detoxification role, as it shows substrate specificity toward toxic aldehydes such as hydroxynonenal (HNE), methyl glyoxale and 3-deoxyglucosone, which arise in large quantities from pathological conditions connected with oxidative stress, as in hyperglycemia.[21] Both ALR1 and ALR2 belong to the aldo-keto reductase (AKR) superfamily, and thus, share a common functional role and the highest structural homology, with 51% identity in their amino acid sequences. The least conserved residues are located at the C-terminal end of the proteins in a region lining the hydrophobic pocket of the active site called the "specificity pocket". This is responsible for substrate and inhibitory specificity in AKRs[22] and can be usefully exploited for the design of selective aldose reductase inhibitors (ARIs).

The limited efficacy of currently known ARIs is generally attributed to pharmacokinetic problems due to their absorption, distribution, metabolism, and excretion properties, but it may also be related to the post-translational modification of ALR2 activity, which is caused by the hyperglycemia-induced oxidative stress. This modification involves oxidation of a critical active cysteine thiol (C298), which regulates both substrate and inhibitor binding. The resulting oxidized form of ALR2 shows an increase in K_m for aldehyde substrates and a marked reduction in sensitivity to ARIs. If a large fraction of the enzyme undergoes conversion to the activated form, the therapeutic

effectiveness of such compounds is largely compromised.[23,24] Therefore, the development of more specific, clinically effective therapies to prevent long-term diabetic complications should necessarily combine ARIs and antioxidants to keep the enzyme in the reduced form. Furthermore, given the extensive data showing the detoxification role of ALR2 against oxidative stress,[25] the concurrent administration of antioxidants can counterbalance its inhibition.

Intrigued by this challenge, we directed our well-known interest in the ARI field[26−29] toward the identification of a novel chemical class capable of combining a good ALR2 inhibitory efficacy with antioxidant properties.

A thorough survey of pertinent literature revealed that the only compounds described with this dual activity are flavonoids. Since the mid-1970s, many papers have appeared reporting extensive structure−activity relationships (SARs) for naturally occurring and synthetic flavonoids. However, none of them provided compounds useful for clinical development. Sometimes they lack appreciable dual efficacy, as compounds exerting significant antioxidant properties show poor ALR2 inhibitory activity or vice versa. In the majority of cases, however, flavonoids possess an inadequate therapeutic index, as they show a broad spectrum of activity.[30−33]

On the basis of these data, we focused our attention on the 2-phenyl-pyrido[1,2-*a*]pyrimidin-4-one (PPP) scaffold, which is a bioisoster of the flavone nucleus, with the aim of developing a novel class of potent and selective ALR2 inhibitors structurally related to flavonoids endowed with antioxidant properties. Herein we present the synthesis and the extensive biological evaluation of a number of derivatives substituted in positions 2, 6, and 9 of the PPP nucleus. Docking simulations of the most active compounds into the human ALR2 binding site were also carried out to rationalize the SARs observed and to guide, perspectively, the design of new analogues.

Chemistry

The synthesis of the title compounds was performed as outlined in Scheme 1. Inhibitors **10**−**12**, **15**−**17**, **20**−**22**, and **25**−**27** were obtained in a one-step reaction by condensing the appropriate 2-aminopyridine **1**−**3** with the suitable β-keto ester **4**−**9** in the presence of polyphosphoric acid (PPA) at 100 °C, following a procedure previously reported for the synthesis of the 4-oxo-4*H*-pyrido[1,2-*a*]pyrimidine ring system.[34]

The starting β-keto esters **7**−**9**, with the exception of the commercially available ones **4**−**6**, were prepared in accordance with a literature procedure[35] involving acylation of Meldrum's acid with the appropriate acyl chloride, followed by ethanolysis of the resulting acylated intermediate.

Inhibitors **13**, **14**, **18**, **19**, **23**, **24**, **28**, and **29** were obtained in good yields from the corresponding methoxy derivatives **11**, **12**, **16**, **17**, **21**, **22**, **26**, and **27** by ether cleavage performed with boron tribromide in a dichloromethane solution.[36]

Results and Discussion

Biological Evaluation. The aim of our research project was to identify potent and selective ARIs endowed with antioxidant properties. All the compounds synthesized were, therefore, tested for efficacy against ALR2 and selectivity for ALR1. Their antioxidant properties were also verified. Tables 1 and 2 list the results of these biological evaluations.

We started our investigation by synthesizing the pyrido[1,2-*a*]pyrimidin-4-one compound **10** and its derivatives, **11**−**14**, bearing methoxy or hydroxyl groups in position 3 or 4 of the 2-phenyl ring. In this series of compounds, only **13** and **14**

Scheme 1. Synthesis of Pyrido[1,2-*a*]pyrimidine Derivatives **10**−**29**

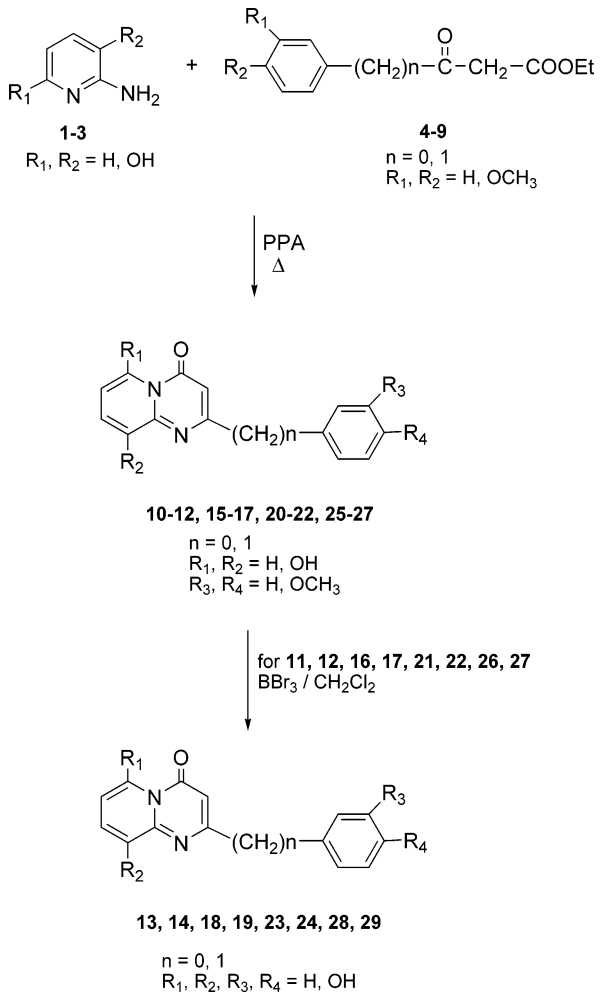

showed any appreciable ALR2 inhibitory activity. In particular, derivative **13**, bearing a 4-hydroxyl group, inhibited ALR2, with an IC_{50} value in the micromolar range (IC_{50} 4.56 μM), thus exhibiting a 2-fold gain in efficacy with respect to quercetin, our starting reference compound. As the pK_a value of **13** (pK_a = 7.60) approaches the pH value of the enzymatic assay, this compound probably acts in its anionic form, as usually occurs with the inhibitors of ALR2. The insertion of an additional hydroxyl group, as in **14**, determines an increase in the acidity of the resulting compound (pK_a = 6.80) and a more favorable interaction with the enzyme anion binding site. Actually, **14** shows a 7-fold increase in the inhibitory potency when compared with **13**, and a 12-fold increase with respect to the reference standard quercetin, with an IC_{50} value in the submicromolar range (IC_{50} 0.67 μM). The lack of activity of compound **10**, which is devoid of hydroxy substituents, as well as that of the methoxylated compounds **11** and **12**, in which proton dissociation is prevented, corroborates the hypothesized interaction of the PPP derivatives **13** and **14** with the enzyme active site.

To verify the importance of the hydroxy substitution on the heterocyclic scaffold, we initially continued our studies by synthesizing derivatives **15**−**19**, which bear this group in position 6 of the core. Consistently with the previously described series, the preferred substitution patterns appeared to be the 4-hydroxy and the 3,4-dihydroxy ones. Compounds **18** and **19** proved to be extremely potent, with IC_{50} values of 0.42 μM and 0.10 μM, respectively. Moreover, they both show an appreciable increase in inhibitory potency, specifically of 11-

Table 1. ALR2 Inhibition Data of Pyrido[1,2-*a*]pyrimidine Derivatives **10**−**29**

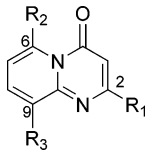

N	R_1	R_2	R_3	ALR2 IC_{50}[a] (μM)	ALR1 IC_{50}[a] (μM)
10	C_6H_5	H	H	>10 μM	>10 μM
11	C_6H_4-4-OCH_3	H	H	>10 μM	>10 μM
12	C_6H_3-3,4-diOCH_3	H	H	>10 μM	>10 μM
13	C_6H_4-4-OH	H	H	4.56 (3.62−5.47)	>10 μM
14	C_6H_3-3,4-diOH	H	H	0.67 (0.52−0.83)	>10 μM
15	C_6H_5	OH	H	10 (7.40−12.1)	>10 μM
16	C_6H_4-4-OCH_3	OH	H	0.74 (0.59−0.89)	>10 μM
17	C_6H_3-3,4-diOCH_3	OH	H	100 (79.1−111.5)	>10 μM
18	C_6H_4-4-OH	OH	H	0.42 (0.36−0.52)	>10 μM
19	C_6H_3-3,4-diOH	OH	H	0.10 (0.077−0.13)	>10 μM
20	CH_2-C_6H_5	OH	H	55 (42.2−65.6)	>10 μM
21	CH_2-C_6H_4-4-OCH_3	OH	H	>10 μM	>10 μM
22	CH_2-C_6H_3-3,4-diOCH_3	OH	H	>10 μM	>10 μM
23	CH_2-C_6H_4-4-OH	OH	H	44 (32.2−55.2)	>10 μM
24	CH_2-C_6H_3-3,4-diOH	OH	H	12 (9.30−14.95)	>10 μM
25	C_6H_5	H	OH	>10 μM	>10 μM
26	C_6H_4-4-OCH_3	H	OH	>10 μM	>10 μM
27	C_6H_3-3,4-diOCH_3	H	OH	>10 μM	>10 μM
28	C_6H_4-4-OH	H	OH	2.07 (1.59−2.49)	>10 μM
29	C_6H_3-3,4-diOH	H	OH	0.45 0.34−0.56)	>10 μM
quercetin				7.81 (5.47−10.15)	2.32 (2.05−2.78)

[a] IC_{50} (95% CL) values represent the concentration required to produce 50% enzyme inhibition.

fold for **18** and 7-fold for **19**, compared with the parent compounds **13** and **14**. Therefore, it seems reasonable to assume that the hydroxy group on the pyridopyrimidine nucleus, which is involved in a hydrogen bond with the adjacent carbonyl group, widens the planar area of the inhibitor's scaffold, increasing the interaction with the lipophilic amino acid residues surrounding the ALR2 active site. Surprisingly, in this series, also compounds **15**−**17** displayed an appreciable inhibitory activity. Compound **15**, which displays a much higher pK_a value (pK_a = 12.0), is a weak acidic compound that binds to the active site in an undissociated form, seeing that the hydroxy group on the pyrido[1,2-*a*]pyrimidine nucleus is involved in the stable hydrogen bond with the adjacent carbonyl group. This holds true also for compounds **16** and **17**, in which any proton dissociation is prevented. Nevertheless, these three compounds show IC_{50} values in the micromolar/submicromolar range, suggesting that an alternative way of binding to the active site of ALR2 should be achieved. While the insertion of a methoxy lipophilic substituent, as in **16**, increases the interaction with the enzyme (**16**, IC_{50} = 0.74 μM, vs **15**, IC_{50} = 10 μM), an additional methoxy group, as in **17**, is detrimental (**17**, IC_{50} = 100 μM, vs **15**, IC_{50} = 10 μM), probably because a steric clash takes place with the walls of the enzyme hydrophobic cleft.

To explore the effects of increasing the distance between the 2-phenyl ring and the pyridopyrimidine nucleus, a methylene spacer was inserted between them to give derivatives **20**−**24**. This distance appeared to be a crucial element, as the lengthened products were less active than the corresponding **15**−**19**. Also in this series, the presence of the hydroxy substituents, as in **23** (IC_{50} = 44.0) and **24** (IC_{50} = 12.0), conferred the best activity, allowing an effective interaction with the enzyme. In addition, the alternative binding mode hypothesized for **15**−**17** may be shared by the unsubstituted derivative **20**, which preserves ALR2 inhibitory efficacy (IC_{50} = 55 μM). However, in this subseries, the methoxy derivatives **21** and **22** display a lower level of activity, probably because the free rotation of the methylene unit, as well as the wider size of the molecule, disturbs the favorable conformation for interaction with the enzyme.

Finally, we synthesized compounds **25**−**29** to investigate the role of the hydroxy group in position 9 of the heterocyclic nucleus. These derivatives generally displayed parallel SARs to those of the parent compounds **10**−**14**, seeing that compounds **25**−**27**, which are devoid of any phenolic group, are inactive. Compound **25** is a weak acid (pK_a = 10.2) and, consequently, it interacts with ALR2 in an undissociated form. This should hold true also for products **26** and **27**, which are devoid of any efficacy. It therefore seems reasonable to hypothesize that no alternative way of binding to the active site of ALR2 can be achieved by these compounds. On the contrary, the phenolic **28** (IC_{50} = 2.07 μM) and **29** (IC_{50} = 0.45 μM) proved to be the only compounds that possessed an inhibitory activity, like their analogues **13** and **14**. These results demonstrate once more the role of the hydroxyl groups on the 2-phenyl ring in anchoring the PPP derivatives to the catalytic site of ALR2.

All the synthesized compounds were assayed for their ability to inhibit ALR1, but none of them showed any appreciable inhibitory properties (IC_{50} > 10 μM, Table 1); all of them proved to be completely selective inhibitors of ALR2.

The antioxidant properties of the newly synthesized compounds were also investigated. Antioxidants can act at different levels in the cellular oxidative pathway, showing multiple mechanisms of action, including scavenging of, or prevention of the formation of, free radicals. We chose to evaluate activities of pyrido[1,2-*a*]pyrimidin-4-ones by examining their effects on hydroxyl radical-dependent lipoperoxidation induced in rat brain homogenate by the oxidant system Fe(III)/ascorbic acid, which initiates the Fenton reaction. For a proper comparison, two standard references were used: α-tocopherol, which is an endogenous chain-breaking antioxidant[37] that protects cells from diverse actions of ROS by donating its hydrogen atom, and deferoxamine, which is an iron chelator[38] that decreases the

Table 2. Effects of Pyrido[1,2-*a*]pyrimidin-4-one Derivatives, α-Tocopherol, or Deferoxamine on the Production of Thiobarbituric Reactive Substances (TBARS) in Rat Brain Homogenate Treated with the Generating Reactive Oxygen Species Fe(III)-Ascorbic Acid[a]

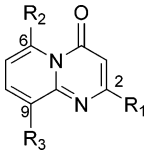

				% of inhibition of control value	
N	R_1	R_2	R_3	100 μM	10 μM
10	C_6H_5	H	H	22.4	10.8
11	C_6H_4-4-OCH_3	H	H	15.1	8.3
12	C_6H_3-3,4-diOCH_3	H	H	18.8	n.a.
13	C_6H_4-4-OH	H	H	23.7	n.a.
14	C_6H_3-3,4-diOH	H	H	71.6	26.6
15	C_6H_5	OH	H	78.1	41.6
16	C_6H_4-4-OCH_3	OH	H	82.8	50.4
17	C_6H_3-3,4-diOCH_3	OH	H	64.7	28.5
18	C_6H_4-4-OH	OH	H	42.4	21.2
19	C_6H_3-3,4-diOH	OH	H	85.9	66.5
20	CH_2-C_6H_5	OH	H	45.7	19.3
21	CH_2-C_6H_4-4-OCH_3	OH	H	42.4	18.9
22	CH_2-C_6H_3-3,4-diOCH_3	OH	H	45.1	25.8
23	CH_2-C_6H_4-4-OH	OH	H	51.4	11.5
24	CH_2-C_6H_3-3,4-diOH	OH	H	89.9	56.7
25	C_6H_5	H	OH	11.9	5.90
26	C_6H_4-4-OCH_3	H	OH	11.5	3.40
27	C_6H_3-3,4-diOCH_3	H	OH	8.80	1.20
28	C_6H_4-4-OH	H	OH	43.2	11.8
29	C_6H_3-3,4-diOH	H	OH	81.5	48.2
α-tocopherol				18.2	
deferoxamine				72.0	

[a] Basal value (rat brain homogenate): TBARS 2.3 ± 0.39 nmol/10 mg wet weight rat brain ($n = 18$). Control (rat brain homogenate plus $FeCl_3$/ascorbic acid): TBARS 7.31 ± 1.15 nmol/10 mg wet weight rat brain ($n = 18$, $P < 0.001$ vs basal value, paired Student's t test). Values are means ± standard errors. Each value is the mean of at least two different determinations performed in triplicate. Absolute values were calculated by performing for each experiment a reference curve using 1,1,3,3-tetramethoxypropane.

concentration of oxidative radicals by inhibiting their iron-catalyzed production.

All the PPP products exhibited significant antioxidant properties. Actually, they inhibited the production of thiobarbituric acid reactive substances (TBARS), an index of lipid peroxidation, with different degrees of efficacy when assayed at a final concentration of 100 μM, as shown in Table 2. In particular, compounds lacking the hydroxy group on the heterocyclic core, namely, **10**−**13**, showed appreciable antioxidant properties, which became excellent for derivative **14**, characterized by the *ortho*-dihydroxy substitution on the 2-phenyl ring. The insertion of the hydroxy group in position 6 of the pyridopyrimidine scaffold, as in compounds **15**−**24**, greatly enhanced antioxidant potency, which still remained marked at 10 μM. Also in this series, the presence of the catechol moiety, as in derivatives **19** and **24**, gave the best activity. On the contrary, shifting the hydroxy substituent to position 9 of the scaffold led to a weakly active series, derivatives **25**−**27**, with the exception of **28** and **29**, in which the presence of the 2-phenyl ring hydroxy groups restored excellent antioxidant properties.

Interestingly, for two of these compounds, namely, **19** and **29**, the high activity as ALR2 inhibitors showed a good correlation with their high activity as ROS scavenging molecules. This additional propriety can ameliorate the pharmacological profile of ALR2 inhibitors, because in this metabolic pathway, an increased quantity of ROS can be produced. It is well accepted that this redox imbalance can worsen diabetes-induced tissue damage at different levels (kidney, eye, vasculature). Furthermore, treatment with antioxidants can keep the enzyme in the reduced form, thus preventing the development of drug resistance following its oxidative modification.

Molecular Modeling. To get a better comprehension of the high ALR2 inhibitory potency of the newly synthesized compounds at a molecular level and to propose a binding mode that explains the above-described SARs, docking experiments and molecular dynamics (MD) simulations were performed. Compounds **16**−**19**, **24**, **28**, and **29** were docked into the binding pocket of the human ALR2/$NADP^+$/tolrestat complex (PDB entry code 2FZD).[39] Docking was carried out using the automated docking program AutoDock,[40] which allows torsional flexibility in the ligand and incorporates an efficient Lamarckian genetic search algorithm together with an empirical free energy function.

Recent crystallographic[22,41] and molecular modeling studies[26−28] have shown that carboxylic acid inhibitors bind to the active site of ALR2 with the acidic function interacting with Y48, H110, and W111, which are three key residues in binding and catalysis.[42,43] Thus, for inhibitors **13** and **14**, the acidic nature of the hydroxyls in the 4 (pK_a 7.60) or 3 and 4 positions (pK_a 6.80) of the pendant phenyl ring is fundamental to the inhibition of ALR2. Indeed, the lack of these hydroxyls, as well as their methylation, which prevents dissociation, leads to completely inactive (**10**−**12**, **21**, **22**, **25**−**27**) or scarcely active (**15**, **17**, **20**) compounds, with the exclusion of **16**. These findings are a clear indication that 4-hydroxy and 3,4-dihydroxy derivatives exert their inhibitory activity toward ALR2 in their anionic dissociated form and that the anionic form produced by dissociation of these hydroxyls could resemble the carboxylate function of carboxylic acid inhibitors. For this reason, inhibitors **18**, **19**, **24**, **28**, and **29** were considered as dissociated (anionic) in the docking and MD simulations. Moreover, theoretical and experimental structures of several 5-hydroxyflavones[44−46] revealed the presence of an intramolecular H-bond, with formation of a six-membered ring involving the 5-OH and 4-C═O groups. For this reason, during the docking of compounds **16**−**19** and **24**, we blocked the torsions involved in this intramolecular bond to prevent the loss of this interaction.

The 50 independent docking runs performed for each ligand usually converged to a small number of different clusters ("clusters" of results differing by less than 1.5 Å rmsd). Generally, the top clusters (i.e., those with the most favorable ΔG_{bind}) were also associated with the highest frequency of occurrence, suggesting a good convergence of the search algorithm. Docking results of the top two clusters, ranked according to the total docking energy ΔG_{bind}, are summarized in Table 3.

Docking of **18**, **19**, **28**, and **29** into the ALR2 crystal structure revealed a very clear preference for two prevailing positions in the binding pocket; these are designated binding orientations A and B, as shown in Figure 1. Interestingly, both results are located in the active site and occupy the same spatial position as the crystallized inhibitor tolrestat.

The top-ranking results, corresponding to orientation A, have their dissociated 4-hydroxyls or 3,4-dihydroxyls placed within the anion binding site, where they make charge-assisted H-bonds with the O^{η} hydrogen of catalytic Y48, while the pyridopyrimidine nucleus is hosted in the specificity pocket. In this position, the six-membered ring intramolecular H-bond formed between the 5-OH and the 4-C═O of the pyridopyrimidine

Table 3. Results of 50 Independent Docking Runs for Each Ligand[a]

cmpd	cluster	orientation	f_{occ}	ΔG_{bind}
16	1	A	13	−9.7
	2		5	−9.1
18	1	A	38	−10.7
	2	B	5	−10.5
19	1	A	23	−10.8
	2	B	10	−10.2
28	1	A	38	−10.7
	2	B	12	−10.4
29	1	A	27	−10.8
	2	B	19	−10.5

[a] The number of results contained in the top two clusters is given by the frequency of occurrence, f_{occ}; ΔG_{bind} is the estimated free energy of binding for the top two clusters and is given in kcal/mol.

nucleus in **19** (Figure 1a) and the 9-OH group in **29** (Figure 1c) point toward the bottom of the specificity pocket. Interestingly, the second-ranking results, which correspond to orientation B, resemble the top ones, except for the pyridopyrimidine nucleus, which is found to rotate by 180 degrees so as to project the six-membered ring intramolecular H-bond (Figure 1b) and the 9-OH (Figure 1d) toward the top of the specificity pocket.

Two prevailing binding positions are also found regarding inhibitor **16**, as can be seen in Figure 2a, and the first (ΔG_{bind} = −9.7 kcal/mol, found 5 times out of 50) closely resembles the above-described binding orientation A, with the OCH_3 oxygen in the 4 position of the pendant phenyl ring involved in two H-bonds with both Y48 O^{η} and H110 $N^{\epsilon 2}$ hydrogens, and the pyridopyrimidine nucleus placed in the specificity pocket, with the six-membered ring intramolecular H-bond pointing toward the bottom of the pocket. A significant alternative to this position is given by the second-ranked solution (ΔG_{bind} = −9.1 kcal/mol, found 13 times out of 50), which places the pyridopyrimidine nucleus in the ALR2 catalytic site and the pendant phenyl ring inside the specificity pocket (Figure 2b). This position allows the formation of two H-bonds: the first between the OCH_3 oxygen in the 4 position of the pendant phenyl ring and the OH hydrogen of T113 and the second one between the 4-C═O oxygen of the pyridopyrimidine nucleus and the W20 $N^{\epsilon 1}$ hydrogen. These results are in agreement with the SAR data, showing that although **16** is a weak acidic compound, it is still able to inhibit ALR2, with an IC_{50} of 0.74 μM.

To elucidate the reasons for the slight decrease in ALR2 inhibitory activity of the lengthened compounds **20**−**24**, the docking of **24** was carried out. The molecule occupies the same space as **19** in its position A (ΔG_{bind} = −10.9 kcal/mol, found 41 times out of 50), with the hydroxyl in position 4 of the pendant phenyl ring involved in a H-bond with Y48 and the pyridopyrimidine system located within the specificity pocket. However, the degree of dissociation of the 4-hydroxyl of **24** is reasonably lower than that of the corresponding hydroxyl of **19** as a result of the methylene spacer that breaks the conjugation between the pyridopyrimidine moiety and the 3,4-dihydroxy phenyl group. This effect decreases the Coulombic component of the H-bond formed between **24** and Y48 and explains the lower ALR2 inhibitory activity of **23** and **24** in comparison with that of **18** and **19**, which form a charge-reinforced H-bond with the Y48 side chain.

In the case of the scarcely active inhibitor **17**, the automated docking calculations did not converge toward a single binding position. From a visual inspection of the **17**/ALR2 complex, it seems clear that the presence of the two methyl groups in the 3 and 4 positions of the pendant phenyl ring increases the steric hindrance inside the binding cavity and changes the optimal binding mode of the ligand, thus decreasing the relative stability of the complex. This may be the reason for the reduced ALR2 inhibitory activity of **17**.

As shown in Table 3, AutoDock unambiguously predicted a preference for binding orientation A only for **19**, whereas for inhibitors **18**, **28**, and **29**, the difference between the estimated free energy of binding for the two orientations A and B was lower than 0.5 kcal/mol. Thus, AutoDock was not able to indicate the preferred orientation for ALR2.

As AutoDock only treats the ligand in a flexible way, an exhaustive protocol of MD simulations was applied, both to relax the inhibitor/ALR2/$NADP^+$ complexes and to evaluate the dynamic behavior of the systems at 300 K. We hypothesized that this procedure might eventually lead us to assess the feasibility of the binding modes identified by AutoDock. For this purpose, 1.2 ns of MD simulations were carried out on the complexes formed between ALR2 and the two prevailing docking positions A and B found for **19** and **29**, chosen as representative members of the whole series.

Chemico-physical parameters, such as temperature, density, potential, and total energy, monitored during the MD simulations, reached stable values for all the complexes after a few hundred picoseconds. Monitoring of the progression of the root-mean-square deviation (rmsd) of the coordinates of the Cα atoms with respect to the initial structure revealed a highly unstable behavior in the complexes formed between ALR2 and both B orientations of **19** (5.7 Å) and **29** (11.7 Å), whereas this behavior was much more stable in the complexes formed between ALR2 and both A orientations of **19** (1.1 Å) and **29** (1.2 Å). This indicated that the overall architectures of the macromolecular complexes were preserved for the whole duration of the simulations. Next, the relative dynamic stability of the A and B orientations of **19** and **29** was monitored by computing the rmsd of the ligands relative to their initial docked position and by monitoring enzyme/ligand hydrogen bond distance time series. Interestingly, some representative interacting distances between the inhibitors analyzed and the ALR2 residues were much more stable for the A binding modes than the B ones. In particular, the interaction between the dissociated 3,4-dihydroxyls of both **19** and **29** with the catalytic residues Y48, H110, and W111 was far more stable for A orientations with respect to B ones throughout the MD simulations. Binding position A of the two inhibitors showed a tendency to fluctuate within the binding site, remaining firmly anchored to certain ALR2 amino acids. These results clearly show that orientation A was dynamically more stable during the MD simulations. This was further confirmed by analyzing the rmsd value of the ligand atoms between the starting and the last MD conformation. Actually, this was as small as 2.2 Å for **19** and 2.1 Å for **29**.

By contrast, position B of the two inhibitors showed a remarkably different behavior; during MD simulation, the ligand/ALR2/$NADP^+$ complexes turned out to be highly unstable, as the ligands left the ALR2 binding site and moved toward the bulk of the solvent already after a few hundred picoseconds. All of the most important interactions with the enzyme residues were lost, and the final rmsd value of the ligand atoms between the starting and the last MD conformations were equal to 6.7 Å for **19** and 10.7 Å for **29**. In this connection, it should be remembered that, during MD simulation, the ligand was allowed to move freely, looking for its best position at the ALR2 binding site, and that the ALR2 binding site is totally exposed to the solvent. Indeed, we added a 20 Å water cap around the binding site, and a consequence of this might have been that position B of **19** and **29**, in which the hydrophilic

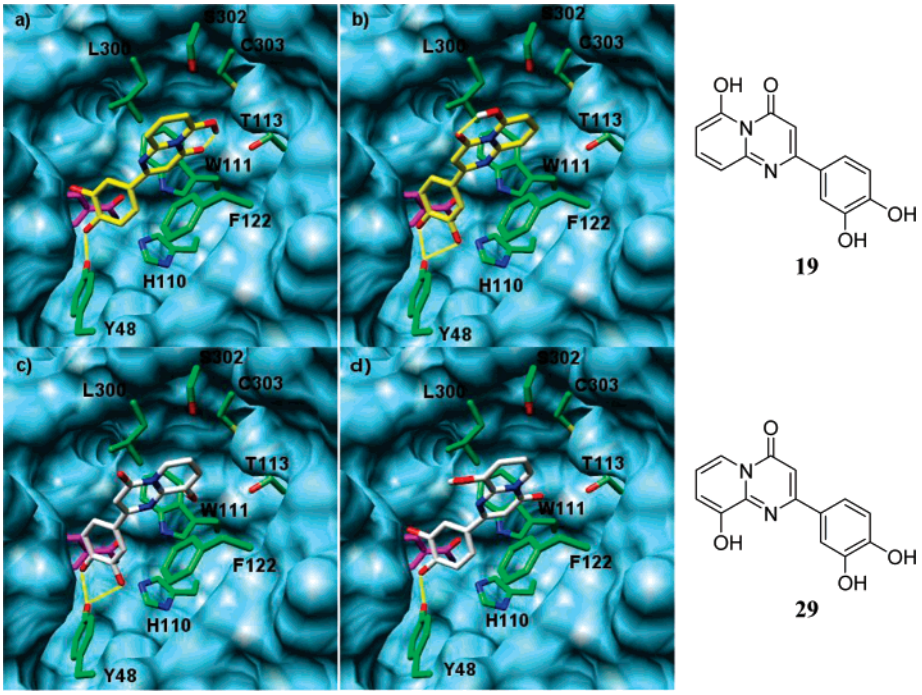

Figure 1. Compounds **19** (yellow) and **29** (white) bound into the active site of human ALR2 represented as a cyan Connolly surface. Binding mode A is depicted at the top for **19** (a) and at the bottom for **29** (c). Binding mode B is illustrated at the top for **19** (b) and at the bottom for **29** (d). Cofactor $NADP^+$ is shown in magenta. The side chains of the key receptor residues in proximity of the docked ligands are highlighted and labeled. Nonpolar hydrogens have been removed for clarity. Hydrogen bonds are represented by yellow lines.

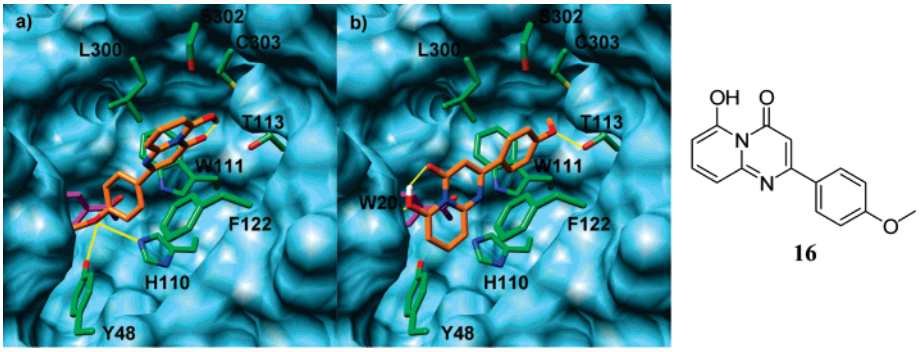

Figure 2. Compound **16** (orange) bound into the active site of human ALR2 represented as a cyan Connolly surface. The top-ranked position is depicted on the left (a) and the second-ranked one is illustrated on the right (b). Cofactor $NADP^+$ is shown in magenta. The side chains of the key enzyme residues in proximity of the docked ligands are highlighted and labeled. Nonpolar hydrogens have been removed for clarity. Hydrogen bonds are represented by yellow lines.

5-OH and 8-OH point toward the bulk of the solvent, tended to escape from the binding site, looking for a more convenient environment in the water.

Figure 3 depicts the MD snapshots characterizing binding mode A of inhibitors **19** and **29** into the ALR2 binding site. As discussed above, the dissociated hydroxyl in the 4 position of the pendant phenyl ring interacts with Y48 and W111 in the **19**/ALR2/$NADP^+$ complex (Figure 3A), while it interacts with Y48 and H110 in the **29**/ALR2/$NADP^+$ complex (Figure 3B). Moreover, the dissociated hydroxyl in position 3 of **19** is within the H-bond distance of the C298 SH group. These results are particularly important because they rationalize the need for dissociated free hydroxyls in positions 3 and 4 of the pendant phenyl ring revealed by SAR data. Furthermore, this corroborates the hypothesis that the dissociated hydroxyls successfully resemble the carboxylate group of several ALR2 inhibitors that have been reported to date.

The pyridopyrimidine system of both inhibitors gets trapped tightly in a hydrophobic pocket formed by residues W79, W111, F115, F122, L124, V130, L300, C303, and W219. It is known that when an inhibitor binds to the ALR2 active site, a conformational change occurs, opening a pocket, designated the specificity pocket, which is localized between F122, W111, L300, and A299.[22] The specific opening of the pocket varies to accommodate each inhibitor, producing an "induced fit". Because the residues lining this pocket are not conserved in ALR1, the interactions are specific for ALR2,[47−49] and as a result, inhibitors with binding interactions in this "specificity pocket" are generally highly selective for ALR2.[22] The finding that **19** and **29** bind in the above-mentioned hydrophobic pocket accounts for the ALR2 selectivity observed for these inhibitors. Of particular interest are the unsuccessful attempts to dock the above compounds into the active site of ALR1, due to steric hindrances between the compounds and the nonconserved residues P301 (L300 in ALR2), T113 (Y115 in ALR2), and R312 (missing in ALR2) from the C-terminal loop, which further explains the high ALR2 selectivity observed for this series of inhibitors.

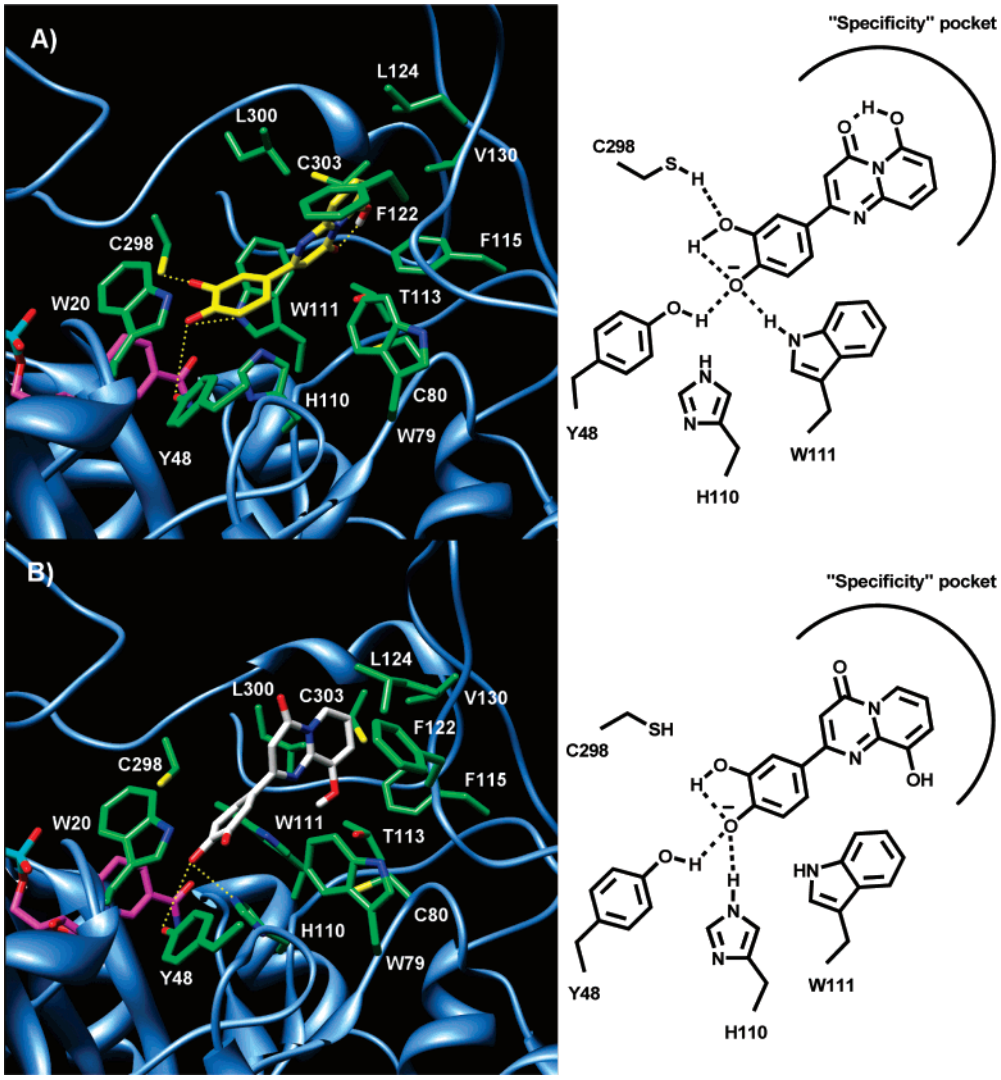

Figure 3. MD snapshots of **19**/ALR2//NADP$^+$ (top, A) and **29**/ALR2//NADP$^+$ (bottom, B) complexes. Only aminoacids located within a 4 Å distance of the bound ligand are displayed and labeled. Carbon atoms of **19** and **29** are yellow and white, respectively. Cofactor NADP$^+$ is shown in magenta. The hydrogen bonds discussed in the text are depicted as dashed yellow lines.

Experimental Section

Chemistry. Melting points were determined using a Reichert Köfler hot-stage apparatus and are uncorrected. Infrared spectra were recorded with a FT-IR spectrometer Nicolet/Avatar in Nujol mulls. Routine nuclear magnetic resonance spectra were recorded in DMSO-d_6 solution on a Varian Gemini 200 spectrometer operating at 200 MHz. Mass spectra were obtained on a Hewlett-Packard 5988 A spectrometer using a direct injection probe and an electron beam energy of 70 eV. Evaporation was performed in vacuo (rotary evaporator). Analytical TLC was carried out on Merck 0.2 mm precoated silica gel aluminum sheets (60 F-254). Elemental analyses were performed by our Analytical Laboratory and agreed with theoretical values to within ±0.4%.

The pyridines 2-aminopyridine, **1**, 2-amino-4-hydroxypyridine, **2**, 2-amino-3-hydroxypyridine, **3**, and the β-keto esters ethyl benzoylacetate, **4**, ethyl 4-methoxybenzoylacetate, **5**, and ethyl 3,4-dimethoxybenzoylacetate, **6**, used to obtain the target inhibitors, were from Aldrich and Fluka. The following compounds were prepared in accordance with a reported procedure: ethyl 3-oxo-4-phenylbutanoate,[50] **7**, ethyl 4-(4-methoxyphenyl)-3-oxobutanoate,[50] **8**, and ethyl 4-(3,4-dimethoxyphenyl)-3-oxobutanoate,[51] **9**.

General Procedure for the Synthesis of 2-Phenylpyrido[1,2-*a*]pyrimidin-4-ones 10−12, 6-Hydroxy-2-phenylpyrido[1,2-*a*]-pyrimidin-4-ones 15−17, 2-Benzylpyrido[1,2-*a*]pyrimidin-4-ones 20−22, and 9-Hydroxy-2-phenylpyrido[1,2-*a*]pyrimidin-4-ones 25−27. A mixture of 2-aminopyridine (1−3, 1.00 mmol) and the appropriate β-keto ester (**4**−**9**, 1.50 mmol) in PPA (2.00 g) was heated at 100 °C for 1 h while stirring with a glass stick. The thick syrup thus obtained was slowly poured into crushed ice, and the resulting suspension was neutralized with 5% aqueous sodium hydroxide. The solid precipitate was collected by filtration, washed with water, and recrystallized (Supporting Information, Tables 1 and 2).

General Procedure for the Synthesis of 2-Phenylpyrido[1,2-*a*]pyrimidin-4-ones 13−14, 6-Hydroxy-2-phenylpyrido[1,2-*a*]-pyrimidin-4-ones 18−19, 2-Benzylpyrido[1,2-*a*]pyrimidin-4-ones 23−24, 9-Hydroxy-2-phenylpyrido[1,2-*a*]pyrimidin-4-ones 28−29. A solution of boron tribromide (0.47 mL, 5.00 mmol) in 3 mL of anhydrous dichloromethane was added dropwise to a well-stirred solution of the appropriate methoxy derivative (**14**−**21**, 1.00 mmol) in 10 mL of anhydrous dichloromethane, cooled at −10 °C. Once the addition was complete, the reaction mixture was allowed to warm to room temperature and maintained under stirring until the disappearance of the starting material (10−24 h, TLC analysis). The suspension was then carefully poured into crushed ice, and the solid precipitate was collected by filtration, washed with water, and recrystallized (Supporting Information, Tables 1 and 2).

Biology. Materials and Methods. ALR2 and ALR1 were obtained from Sprague−Dawley albino rats, 120−140 g, b.w., supplied by Harlan Nossan, Italy. To minimize cross-contamination between ALR2 and ALR1 in the enzyme preparation, rat lens, in which ALR2 is the predominant enzyme, and kidney, where ALR1

shows the highest concentration, were used for the isolation of ALR2 and ALR1, respectively.

Pyridine coenzyme, D,L-glyceraldehyde, sodium D-glucuronate, quercetin, ascorbic acid, ferric chloride, thiobarbituric acid, 1,1,3,3-tetramethoxypropane, α-tocopherol, and deferoxamine were from Sigma-Aldrich. All other chemicals were of reagent grade.

Enzyme Preparation. Aldose Reductase. A purified rat lens extract was prepared in accordance with the method of Hayman and Kinoshita,[52] with slight modifications. Lenses were quickly removed from rats following euthanasia and were homogenized (Glas-Potter) in three volumes of cold deionized water. The homogenate was centrifuged at 12 000 rpm at 0−4 °C for 30 min. Saturated ammonium sulfate solution was added to the supernatant fraction to form a 40% solution, which was stirred for 30 min at 0−4 °C and then centrifuged at 12 000 rpm for 15 min. Following this same procedure, the recovered supernatant was subsequently fractionated with saturated ammonium sulfate solution using first a 50% and then a 75% salt saturation. The precipitate recovered from the 75% saturated fraction, possessing ALR2 activity, was redissolved in 0.05 M NaCl and dialyzed overnight in 0.05 M NaCl. The dialyzed material was used for the enzymatic assay.

Aldehyde Reductase. Rat kidney ALR1 was prepared in accordance with a previously reported method.[53] Kidneys were quickly removed from normal killed rats and homogenized (Glas-Potter) in three volumes of 10 mM sodium phosphate buffer, pH 7.2, containing 0.25 M sucrose, 2.0 mM EDTA dipotassium salt, and 2.5 mM β-mercaptoethanol. The homogenate was centrifuged at 12 000 rpm at 0−4 °C for 30 min and the supernatant was subjected to a 40−75% ammonium sulfate fractionation, following the same procedure previously described for ALR2. The precipitate obtained from the 75% ammonium sulfate saturation, possessing ALR1 activity, was redissolved in 50 volumes of 10 mM sodium phosphate buffer, pH 7.2, containing 2.0 mM EDTA dipotassium salt and 2.0 mM β-mercaptoethanol and was dialyzed overnight using the same buffer. The dialyzed material was used in the enzymatic assay.

Enzymatic Assays. The activity of the two test enzymes was determined spectrophotometrically by monitoring the change in absorbance at 340 nm, which is due to the oxidation of NADPH catalyzed by ALR2 and ALR1. The change in pyridine coenzyme concentration/min was determined using a Beckman DU-64 kinetics software program (Solf Pack TM Module).

ALR2 activity was assayed at 30 °C in a reaction mixture containing 0.25 mL of 10 mM d,L-glyceraldehyde, 0.25 mL of 0.104 mM NADPH, 0.25 mL of 0.1 M sodium phosphate buffer (pH 6.2), 0.1 mL of enzyme extract, and 0.15 mL of deionized water in a total volume of 1 mL. All the above reagents, except D,L-glyceraldehyde, were incubated at 30 °C for 10 min; the substrate was then added to start the reaction, which was monitored for 5 min. Enzyme activity was calibrated by diluting the enzymatic solution to obtain an average reaction rate of 0.011 ± 0.0010 absorbance units/min for the sample.

ALR1 activity was determined at 37 °C in a reaction mixture containing 0.25 mL of 20 mM sodium D-glucuronate, 0.25 mL of 0.12 mM NADPH, 0.25 mL of dialyzed enzymatic solution, and 0.25 mL of 0.1 M sodium phosphate buffer (pH 7.2) in a total volume of 1 mL. The enzyme activity was calibrated by diluting the dialyzed enzymatic solution to obtain an average reaction rate of 0.015 ± 0.0010 absorbance/min for the sample.

Enzymatic Inhibition. The inhibitory activity of the newly synthesized compounds against ALR2 and ALR1 was assayed by adding 0.1 mL of the inhibitor solution to the reaction mixture described above. All the inhibitors were solubilized in water and the solubility was facilitated by adjustment to a favorable pH. After complete solution, the pH was readjusted to 7. To correct for the nonenzymatic oxidation of NADPH and for absorption by the compounds tested, a reference blank containing all the above assay components except the substrate was prepared. The inhibitory effect of the new derivatives was routinely estimated at a concentration of 10^{-4} M. Those compounds found to be active were tested at additional concentrations between 10^{-5} and 10^{-8} M. The determination of the IC_{50} values was performed by linear regression analysis of the log−dose response curve, which was generated using at least four concentrations of the inhibitor causing an inhibition between 20% and 80%, with two replicates at each concentration. The 95% confidence limits (95% CL) were calculated from *t* values for *n*-2, where *n* is the total number of determinations.

Thiobarbituric Acid Reagent Substance Assay. Freshly isolated rat brain was homogenized in 10% (w/v) phosphate buffer, pH 7.4. $FeCl_3$ (20 μM) and 100 μM ascorbic acid (final concentrations) were added to 100 μL of rat brain homogenate, in the absence or presence of the test compounds or reference scavenger molecules, and were diluted to 1 mL with phosphate buffer, pH 7.4. Samples were incubated for 30 min at 37 °C in a water bath under slight stirring, and were then mixed with 0.5 mL of thiobarbituric acid (1% w/v in 0.05 N NaOH) and 0.5 mL of 25% v/v HCl. The mixture was boiled for 10 min and, after cooling in an ice-cold water bath, extraction was performed with 3 mL of n-butanol. After liquid-phase separation (centrifugation at 2000 g for 10 min), the absorbance of the pink organic phase was spectrophotometrically evaluated at 532 nm and TBARS was expressed as nmoles of malondialdehyde (MDA)/10 mg of rat brain tissue (wet weight), using a curve with 1,1,3,3-tetramethoxypropane as the standard reference.[54]

Computational Chemistry. Molecular modeling and graphics manipulations were performed using the SYBYL[55] and UCSF CHIMERA software packages,[56] running them on a Silicon Graphics Tezro R16000 workstation. Model building of inhibitors **16**−**19**, **28**, and **29** was accomplished by using the TRIPOS force field[57] available within SYBYL. Energy minimizations and MD simulations were performed with the AMBER 8.0 program,[58] using the parm99 force field.[59]

Docking Simulations. Docking was performed with version 3.05 of the program AutoDock,[40] which combines a rapid energy evaluation through precalculated grids of affinity potentials with a variety of search algorithms to find suitable binding positions for a ligand on a given protein. While the protein is required to be rigid, the program allows torsional flexibility in the ligand.

Ligand Setup. Molecular models of compounds **16**−**19**, **28**, and **29** were constructed using standard bond lengths and bond angles of the SYBYL fragment library. Hydroxyls in the 3 and 4 position of the ligand pendant phenyl ring were taken as dissociated, on account of the low pK_a value of these groups. Geometry optimizations were realized with the SYBYL/MAXIMIN2 minimizer by applying the BFGS (Broyden, Fletcher, Goldfarb and Shannon) algorithm[60] and setting an rms gradient of the forces acting on each atom of 0.05 kcal/mol Å as the convergence criterion. Atomic charges were assigned using the Gasteiger−Marsili formalism,[61] which is the type of atomic charge used in calibrating the AutoDock empirical free energy function.

Protein Setup. The crystal structure of human ALR2 complexed with tolrestat (PDB entry code 2FZD),[39] recovered from Brookhaven Protein Database,[62] was used in the docking experiments.

Although the inhibition assays on our compounds were conducted on rat ALR2, the use of the human ALR2 crystal structure for docking is justified by the following facts: (i) the crystal structure of rat ALR2 is unknown; (ii) the human and rat sequences of this enzyme are characterized by 81% identity and 89% homology;[63] (iii) all active-site residues, including those of the specificity pocket, are largely conserved across the ALR2 isoforms so far sequenced.

The structure was set up for docking as follows: polar hydrogens were added by using the BIOPOLYMERS module within the SYBYL program (residues Arg, Lys, Glu, and Asp were considered ionized, while all His were considered to be neutral by default with hydrogen atoms fixed at the $N^{\epsilon 2}$ atom), Kollman united atom partial charges were assigned, and all waters were removed.

AutoDock Docking. Docking of compounds **16**−**19**, **28**, and **29** to ALR2 was carried out using the empirical free energy function and the Lamarckian genetic algorithm, applying a standard protocol with an initial population of 50 randomly placed individuals, a maximum number of 1.5×10^6 energy evaluations, a mutation rate of 0.02, a crossover rate of 0.80, and an elitism value of 1.

Proportional selection was used, where the average of the worst energy was calculated over a window of the previous 10 generations. For the local search, the so-called pseudo Solis and Wets algorithm was applied, using a maximum of 300 iterations. The probability of performing local search on an individual in the population was 0.06, and the maximum number of consecutive successes or failures before doubling or halving the local search step size was 4.

Fifty independent docking runs were carried out for each ligand. Results differing by less than 1 Å in positional rmsd were clustered together and were represented by the result with the most favorable free energy of binding (ΔG_{bind}). Finally, the compounds were set up for docking with the help of AutoTors, the main purpose of which is to define the torsional degrees of freedom to be considered during the docking process. All torsion angles for each compound were considered flexible. Solvation parameters were added to the final protein file by using the ADDSOL utility of AutoDock. The grid maps representing the proteins in the actual docking process were calculated with AutoGrid. The grids (one for each atom type in the ligand plus one for electrostatic interactions) were chosen to be sufficiently large to include not only the active site but also significant portions of the surrounding surface. The dimensions of the grids were thus 30 Å × 30 Å × 30 Å, with a spacing of 0.375 Å between the grid points.

MD Simulations. All MD simulations were performed using the SANDER module in the AMBER suite of programs. An all-atom representation of the system was used, employing the Cornell et al.[59] force field to assign parameters for the standard amino acids. General AMBER force field (GAFF) parameters were assigned to ligands and $NADP^+$ cofactor, while the partial charges were calculated using the AM1-BCC method as implemented in the ANTECHAMBER suite of AMBER. **19**/ALR2/$NADP^+$ and **29**/ALR2/$NADP^+$ complexes were solvated with a water cap (TIP3P)[64] up to 30 Å from the inhibitor. A "belly" region of 15 Å was then defined around the ligand. During the simulations, those "belly" atoms that are less than 15 Å from the ligand were allowed to move, while all atoms beyond 15 Å were held rigid.

The initial complexes were energy-minimized for 10 500 steps using combined steepest descent and conjugate gradient methods until a convergence value of 0.001 kcal/Å·mol. Upon minimization, the water cap was equilibrated for 10 picoseconds (ps) to allow cavities in the protein to become solvated. The entire "belly" region was then equilibrated for 100 ps with the system warmed to 300 K over the initial 0.2 ps equilibrated at 300 K for another 25 ps. A subsequent production run was performed at a constant temperature of 300 K and a constant pressure of 1 atm, giving a total simulation time of 1.2 ns. The time interval was set to 2 fs. The SHAKE method[65] was applied to constrain all of the covalent bonds involving hydrogen atoms. During the simulation, nonbonded cutoffs were set to 12 Å. Neither constraints nor restraints were applied to the complexes during the MD simulations, allowing the inhibitor molecule to move freely between the protein surface and the bulk of the solvent. The CARNAL module of AMBER was used to check some structural properties (rmsd, hydrogen bonds). The hydrogen bond criterion was a maximum donor−acceptor distance of 3.5 Å and a minimum donor−proton−acceptor angle of 120°.

Supporting Information Available: Tables 1 and 2, including physical and spectral data of compounds **11**, **13**, **15**−**17**, and **19**−**29**, and analytical data of compounds **11**, **13**, **15**−**17**, and **19**−**29**. This material is available free of charge via the Internet at http://pubs.acs.org.

References

(1) King, H.; Aubert, R. E.; Herman, W. H. Global Burden of Diabetes, 1995−2025. Prevalence, Numerical Estimates, and Projection. *Diabetes Care* **1998**, *21*, 1414−1431.

(2) Boyle, J. P.; Honeycutt, A. A.; Venkat Narayan, K. M.; Hoerger, T. J.; Geiss, L. S.; Chen, H.; Thompson, T. J. Projection of Diabetes Burden Through 2025. *Diabetes Care* **2001**, *24*, 1936−1940.

(3) Wild, S.; Roglic, G.; Green, A.; Sicree, R.; King, H. Global Prevalence of Diabetes: Estimates for the Year 2000 and Projections for 2030. *Diabetes Care* **2004**, *27*, 1047−1053.

(4) Zimmet, P. Z.; Alberti, K. G. M. M.; Shaw, J. Global and Societal Implications of the Diabetic Epidemic. *Nature* **2001**, *414*, 782−787.

(5) American Diabetes Association. Economic costs of Diabetes in the U.S. in 2002. *Diabetes Care* **2003**, *26*, 917−932.

(6) Brownlee, M. Biochemical and Molecular Cell Biology of Diabetic Complications. *Nature* **2001**, *414*, 813−820.

(7) Altan, V. M. The Pharmacology of Diabetic Complications. *Curr. Med. Chem.* **2003**, *10*, 1317−1327.

(8) Knowler, W. C.; Narayan, K. M. V.; Hanson, R. L.; Nelson, R. G.; Bennett, P. H.; Tuomilehto, J.; Schersten, B.; Pettitt, D. J. Preventing Non-Insulin-Dependent Diabetes Mellitus. *Diabetes* **1995**, *22*, 483−488.

(9) The Diabetes Prevention Program Research Group. The Diabetes Prevention Program: Design and Methods for a Clinical Trial in the Prevention of Type 2 Diabetes. *Diabetes Care* **1999**, *22*, 623−634.

(10) The Diabetes Control and Complications Trial Research Group. The Effect of Intensive Treatment of Diabetes on the Development and Progression of Long-Term Complications in Insulin-Dependent Diabetes Mellitus. *N. Engl. J. Med.* **1993**, *329*, 977−986.

(11) U. K. Prospective Diabetes Study Group. Intensive Blood-Glucose Control with Sulfonylureas of Insulin Compared with Conventional Treatment and Risk of Complications in Patients with Type 2 Diabetes (UKPDS 33). *Lancet* **1998**, *352*, 837−853.

(12) Kador, P. F. The role of Aldose Reductase in the Development of Diabetic Complications. *Med. Res. Rev.* **1998**, *8*, 325−352.

(13) Tomlinson, D. R.; Stevens, E. J.; Diemel, L. T. Aldose Reductase Inhibitors and their Potential for the Treatment of Diabetic Complications. *Trends Pharmacol. Sci.* **1994**, *15*, 293−297.

(14) Yabe-Nishimura, C. Aldose Reductase in Glucose Toxicity: A Potential Target for the Prevention of Diabetic Complications. *Pharmacol. Rev.* **1998**, *50*, 21−33.

(15) Williamson, J. R.; Chang, K.; Frangos, M.; Hasan, K. S.; Ido, Y.; Kawamura, T.; Nyengaard, J. R.; van der Enden, M.; Kilo, C.; Tilton, R. G. Hyperglycemic Pseudohypoxia and Diabetic Complications. *Diabetes* **1993**, *42*, 801−813.

(16) Ido, Y.; Williamson, J. R. Hyperglycemic Cytosolic Reductive Stress "Pseudohypoxia": Implications for Diabetic Retinopathy. *Invest. Ophthalmol. Visual Sci.* **1997**, *38*, 1467−1470.

(17) Purves, T.; Middlemas, A.; Agthon, S.; Jude, E. B.; Boulton, A. J.; Fernyhough, P.; Tomlinson, D. R. A Role for Mitogen-Activated Protein Kinases in the Etiology of Diabetic Neuropathy. *FASEB J.* **2001**, *15*, 2508−2514.

(18) Obrosova, I. G.; Li, F.; Abatan, O. I.; Forsell, M. A.; Komjati, K.; Pacher, P.; Szabo, C.; Stevens, M. J. Role of Poly(ADP-ribose)-polymerase Activation in Diabetic Neuropathy. *Diabetes* **2004**, *53*, 711−720.

(19) Joussen, A. M.; Poulaki, V.; Le, M. L.; Koizumi, K.; Esser, C.; Janicki, H.; Scharaermeyer, U.; Kociok, N.; Fauser, S.; Kirchhof, B.; Kern, T. S.; Adamis, A. P. A Central Role for Inflammation in the Pathogenesis of Diabetic Retinopathy. *FASEB J.* **2004**, *18*, 1450−1452.

(20) Chung, S. S.; Chung, S. K. Genetic Analysis of Aldose Reductase in Diabetic Complications. *Curr. Med. Chem.* **2003**, *10*, 1375−1387.

(21) Carper, D.; Wiston, G.; Nishimura, C.; Graham, C.; Watanabe, K.; Fuji, Y.; Hayaishi, H.; Hayaishi, O. A Superfamily of NADPH-Dependent Reductases in Eukaryotes and Prokaryotes. *Exp. Eye Res.* **1988**, *49*, 377−388.

(22) Urzhumtsev, A.; Tete-Favier, F.; Mitscler, A.; Barbanton, J.; Barth, P.; Urzhumgtseva, L.; Biellmann, J. F.; Podjarny, A. D.; Moras, D. A "Specificity" Pocket Inferred from the Crystal Structures of the Complexes of Aldose Reductase with the Pharmaceutically Important Inhibitors Tolrestat and Sorbinil. *Structure* **1997**, *5*, 601−612.

(23) Cappiello, M.; Voltarelli, M.; Cecconi, I.; Vilardo, P. G.; Dal Monte, M.; Marini, I.; Del Corso, A.; Wilson, D. K.; Quiocho, F. A.; Petrash, J. M.; Mura, U. Specifically Targeted Modification of Human Aldose Reductase by Physiological Disulfides. *J. Biol. Chem.* **1996**, *271*, 33539−33544.

(24) Grimshaw, C. E.; Lai, C. J. Oxidized Aldose Reductase: In Vivo Factor, Not In Vitro Artifact. *Arch. Biochem. Biophys.* **1996**, *327*, 89−97.

(25) Srivastava, S. K.; Ramana, K. V.; Bhatnagar, A. Role of Aldose Reductase and Oxidative Damage in Diabetes and the Consequent Potential for Therapeutic Options. *Endocr. Rev.* **2005**, *26*, 380−392.

(26) Da Settimo, F.; Primofiore, G.; Da Settimo, A.; La Motta, C.; Taliani, S.; Simorini, F.; Novellino, E.; Greco, G.; Lavecchia, A.; Boldrini, E. [1,2,4]Triazino[4,3-*a*]benzimidazole Acetic Acid Derivatives: A New Series of Selective Aldose Reductase Inhibitors. *J. Med. Chem.* **2001**, *44*, 4359−4369.

(27) Da Settimo, F.; Primofiore, G.; Da Settimo, A.; La Motta, C.; Simorini, F.; Novellino, E.; Greco, G.; Lavecchia, A.; Boldrini, E. Novel, Highly Potent Aldose Reductase Inhibitors: Cyano-(2-oxo-2,3-dihydroindol-3-yl)-acetic Acid Derivatives. *J. Med. Chem.* **2003**, *46*, 1419−1428.

(28) Da Settimo, F.; Primofiore, G.; La Motta, C.; Sartini, S.; Taliani, S.; Simorini, F.; Marini, A. M.; Lavecchia, A.; Novellino, E.; Boldrini, E. Naphtho[1,2-*d*]isothiazole Acetic Acid Derivatives as a Novel Class of Selective Aldose Reductase Inhibitors. *J. Med. Chem.* **2005**, *48*, 6897−6907.

(29) Da Settimo, F.; Primofiore, G.; La Motta, C.; Salerno, S.; Novellino, E.; Greco, G.; Lavecchia, A.; Laneri, S.; Boldrini, E. Spirohydantoin Derivatives of Thiopyrano[2,3-*b*]pyridin-4(4*H*)-one as Potent In Vitro and In Vivo Aldose Reductase Inhibitors. *Bioorg. Med. Chem.* **2005**, *13*, 491−499.

(30) Kawanishi, K.; Ueda, H.; Moriyasu, M. Aldose Reductase Inhibitors from the Nature. *Curr. Med. Chem.* **2003**, *10*, 1353−1374.

(31) Costantino, L.; Rastelli, G.; Gamberini, M. C.; Vinson, J. A.; Bose, P.; Iannone, A.; Staffieri, M.; Antolini, L.; Del Corso, A.; Mura, U.; Albasini, A. 1-Benzopyran-4-one Antioxidants as Aldose Reductase Inhibitors. *J. Med. Chem.* **1999**, *42*, 1881−1893.

(32) Lim, S. S.; Jung, S. H.; Ji, J.; Shin, K. H.; Keum, S. R. Synthesis of Flavonoids and their Effects on Aldose Reductase and Sorbitol Accumulation in Streptozotocin-Induced Diabetic Rat Tissues. *J. Pharm. Pharmacol.* **2001**, *53*, 653−668.

(33) Matsuda, H.; Morikawa, T.; Toguchida, I.; Yoshikawa, M. Structural Requirements of Flavonoids and Related Compounds for Aldose Reductase Inhibitory Activity. *Chem. Pharm. Bull.* **2002**, *50*, 788−795.

(34) Shur, M.; Israelstam, S. S. The Reaction of Amino Heterocycles with Reactive Esters. I. 2-Aminopyridines. *J. Org. Chem.* **1968**, *33*, 3015−3019.

(35) Oikawa, Y.; Sugano, K.; Yonemitsu, O. Meldrum's Acid in Organic Synthesis. 2. A General and Versatile Synthesis of β-Keto Esters. *J. Org. Chem.* **1978**, *43*, 2087−2088.

(36) Felix, A. M. Cleavage of Protecting Groups with Boron Tribromide. *J. Org. Chem.* **1974**, *39*, 1427−1429.

(37) Burton, G. W.; Ingold, K. U. Vitamin E as an In Vitro and In Vivo Antioxidant. *Ann. N.Y. Acad. Sci.* **1989**, *570*, 7−22.

(38) Kontoghiorghes, G. J. New Chelation Therapies and Emerging Chelating Drugs for the Treatment of Iron Overload. *Expert Opin. Emerging Drugs* **2006**, *11*, 1−5.

(39) Steuber, H.; Zentgraf, M.; Gerlach, C.; Sotriffer, C. A.; Heine, A.; Klebe, G. Expect the Unexpected or Caveat for Drug Designers: Multiple Structure Determinations Using Aldose Reductase Crystals Treated under Varying Soaking and Co-crystallisation Conditions. *J. Mol. Biol.* **2006**, *363*, 174−187.

(40) Morris, G. M.; Goodsell, D. S.; Halliday, R. S.; Huey, R.; Hart, W. E.; Belew, R. K.; Olson, A. J. Automated Docking Using a Lamarckian Genetic Algorithm and an Empirical Binding Free Energy Function. *J. Comput. Chem.* **1998**, *19*, 1639−1662.

(41) Wilson, D. K.; Tarle, I.; Petrash, J. M.; Quiocho, F. A. Refined 1.8 A Structure of Human Aldose Reductase Complexed with the Potent Inhibitor Zopolrestat. *Proc. Natl. Acad. Sci. U.S.A.* **1993**, *90*, 9847−9851.

(42) Bohren, K. M.; Grimshaw, C. E.; Lai, C. J.; Harrison, D. H.; Ringe, D.; Petsko, G. A.; Gabbay, K. H. Tyrosine-48 is the Proton Donor and Histidine-110 Directs Substrate Stereochemical Selectivity in the Reduction Reaction of Human Aldose Reductase: Enzyme Kinetics and Crystal Structure of the Y48H Mutant Enzyme. *Biochemistry* **1994**, *33*, 2021−2032.

(43) Grimshaw, C. E.; Bohren, K. M.; Lai, C. J.; Gabbay, K. H. Human Aldose Reductase: pK of Tyrosine 48 Reveals the Preferred Ionization State for Catalysis and Inhibition. *Biochemistry* **1995**, *34*, 14374.

(44) Etter, M. C.; Lipkowska, Z.; Baer, S.; Barbara, P. F. The Crystal Structures and Hydrogen-Bond Properties of Three 3-Hydroxyflavone Derivatives. *J. Mol. Struct.* **1986**, *144*, 155−167.

(45) Shoja, M. 5-Hydroxyflavone. *Acta Crystallogr., Sect. C* **1990**, *46*, 517−519.

(46) Meyer, M. Ab Initio Study of Flavonoids. *Int. J. Quantum Chem.* **2000**, *76*, 724−732.

(47) El-Kabbani, O.; Wilson, D. K.; Petrash, J. M.; Quiocho, F. A. Structural Features of the Aldose Reductase and Aldehyde Reductase Inhibitor-Binding Sites. *Mol. Vis.* **1998**, *4*, 19−25.

(48) Rees-Milton, K. J.; Jia, Z.; Green, N. C.; Bhatia, M.; El-Kabbani, O.; Flynn, T. G. Aldehyde Reductase: The Role of C-Terminal Residues in Defining Substrate and Cofactor Specificities. *Arch. Biochem. Biophys.* **1998**, *355*, 137−144.

(49) El-Kabbani, O.; Carper, D. A.; McGowan, M. H.; Devedjiev, Y.; Rees-Milton, K. J.; Flynn, T. G. Studies on the Inhibitor-Binding Site of Porcine Aldehyde Reductase: Crystal Structure of the Holoenzyme-Inhibitor Ternary Complex. *Proteins* **1997**, *29*, 186−192.

(50) Svenstrup, N.; Simonsen, K. B.; Thorup, N.; Brodersen, J.; Dehaen, W.; Becher, J. A Pyrazole to Furan Rearrangement. Thermolysis of 5-Azido-4-formylpyrazoles. *J. Org. Chem.* **1999**, *64*, 2814−2820.

(51) Shin, H.; Choi, B. S.; Lee, K. K.; Choi, H-W.; Chang, J. H.; Lee, K. W.; Nam, D. H.; Kim, N. S. Efficient Activation of Zinc: Application of the Blaise Reaction to an Expedient Synthesis of a Statin Intermediate. *Synthesis* **2004**, *16*, 2629−2632.

(52) Hayman, S.; Kinoshita, J. H. Isolation and Properties of Lens Aldose Reductase. *J. Biol. Chem.* **1965**, *240*, 877−882.

(53) Ward, W. H. J.; Sennitt, C.M.; Ross, H.; Dingle, A.; Timmus, D.; Mirrless, D. J.; Tuffin, D. P. Ponalrestat, A Potent and Specific Inhibitor of Aldose Reductase. *Biochem. Pharmacol.* **1990**, *39*, 337−346.

(54) Cantore, M.; Siano, S.; Coronnello, M.; Mazzetti, L.; Franchi-Micheli, S.; Ciuffi, M.; Failli, P. Pirenoxine Prevents Oxidative Effects of Argon Fluoride Excimer Laser Irradiation in Rabbit Corneas: Biochemical, Histological, and Cytofluorimetric Evaluation. *J. Photochem. Photobiol., B.* **2005**, *75*, 34−42.

(55) *SYBYL*, Molecular Modeling System, version 7.1; TRIPOS Assoc., St. Louis, MO.

(56) Huang, C. C.; Couch, G. S.; Pettersen, E. F.; Ferrin, T. E. Chimera: An Extensible Molecular Modeling Application Constructed Using Standard Components. *Pac. Symp. Biocomput.* **1996**, *1*, 724 (http://www.cgl.ucsf.edu/chimera).

(57) Vinter, J. G.; Davis, A.; Saunders, M. R. Strategic Approaches to Drug Design. 1. An Integrated Software Framework for Molecular Modelling. *J. Comput.-Aided Mol. Des.* **1987**, *1*, 31−55.

(58) Case, D. A.; Darden, T. A.; Cheatham, T. E., III; Simmerling, C. L.; Wang, J.; Duke, R. E.; Luo, R.; Merz, K. M.; Wang, B.; Pearlman, D. A.; Crowley, M.; Brozell, S.; Tsui, V.; Gohlke, H.; Mongan, J.; Hornak, V.; Cui, G.; Beroza, P.; Schafmeister, C.; Caldwell, J. W.; Ross, W. S.; Kollman, P. A. *AMBER 8*; University of California: San Francisco, CA, 2004.

(59) Cornell, W. D.; Cieplak, P.; Bayly, C. I.; Gould, I. R.; Merz, K. M., Jr.; Ferguson, D. M.; Spellmeyer, D. C.; Fox, T.; Caldwell, J. W.; Kollman, P. A. A Second Generation Force Field for the Simulation of Proteins, Nucleic Acids, and Organic Molecules. *J. Am. Chem. Soc.* **1995**, *117*, 5179−5197.

(60) Head, J.; Zerner, M. C. A Broyden−Fletcher−Goldfarb−Shannon Optimization Procedure for Molecular Geometries. *Chem. Phys. Lett.* **1985**, *122*, 264−274.

(61) Gasteiger, J.; Marsili, M. Iterative Partial Equalization of Orbital Electronegativity−A Rapid Access to Atomic Charges. *Tetrahedron* **1980**, *36*, 3219−3228.

(62) Bernstein, F. C.; Koetzle, T. F.; Williams, G. J. B.; Meyer, E. F., Jr.; Brice, M. D.; Rodgers, J. R.; Kennard, O.; Shimanouchi, T.; Tasumi, T. The Protein Data Bank: A Computer Based Archival File for Macromolecular Structures. *J. Mol. Biol.* **1977**, *112*, 535−542.

(63) Database searching (SWISS-PROT), sequence alignment, and analysis of rat and human ALR2 sequences were carried out using FASTA (Pearson, W. R. *Proc. Natl. Acad. Sci. U.S.A.* **1988**, *85*, 2444−2448) and BLAST programs (Wang, S.; Pak, Y. *J. Phys. Chem. B* **2000**, *104*, 354−359).

(64) Jorgensen, W. L.; Chandrasekhar, J.; Madura, J. D.; Impey, R. W.; Klein, M. L. Comparison of Simple Potential Functions for Simulating Liquid Water. *J. Chem. Phys.* **1983**, *79*, 926−935.

(65) Hayward, S.; Kitao, A.; Go, N. Harmonicity and Anharmonicity in Protein Dynamics: A Normal-Mode Analysis and Principal Component Analysis. *Proteins* **1995**, *23*, 177−186.

JM070398A